Int. J. Heat Mass Transfer. Vol. 14, pp. 1261–1274. Pergamon Press 1971. Printed in Great Britain

MASS TRANSFER IN TWO-PHASE GAS–LIQUID WAVY FLOW

JANUSZ W. CIBOROWSKI

Department of Chemical Engineering, Institute of Technology, Koszykowa 75, Warsaw, Poland

and

RAJMUND M. RYCHLICKI

Centro Informazioni Studi Esperienze, CISE Via Redecesio 12, Segrate, Milan, Italy

(*Received* 29 *June* 1970 *and in revised form* 3 *November* 1970)

Abstract—Mass transfer in horizontal two-phase gas–liquid wavy flow in the round duct has been investigated.

Correlations of mass transfer coefficients for gas and liquid film resistances were obtained experimentally.

The mass-momentum analogy, based on experimental wavy-surface friction factor data, was utilized to determine the mass-transfer coefficients.

A comparison was made between mass-transfer coefficient experimental data and data obtained by the analogy method.

Some experiments on wave flow dynamics and geometry were also performed.

NOMENCLATURE

A, intersurface area [m^2];
a, heat diffusity [m^2/h];
b, width of water stream [m];
C, specific heat [kcal/kg degree];
c, wave celerity [cm/s];
D, diffusity [m^2/h];
d, diameter; depth of water [m];
E, eddy diffusity [m^2/h];
f, friction factor;
G, gas flowrate [kg/m^2s];
g, gravity, 9·81 m/s^2;
H, Henry's constant [kmol/atm m^3];
h, heat-transfer coefficient [kcal/m^2 h degree];
K, overall mass transfer coefficient [kmol/m^2 h conc. or pressure];
K, equilibrium constant;
k, partial mass transfer coefficient [kmol/m^2 h conc or pressure];
L, liquid flowrate [kg/m^2 s];
l, length [m];
M, molecular weight;
P, overall pressure [atm];
p, partial pressure [atm];
R, volume fraction; gas constant;
T, temperature [degrees];
t, time [s];
u, velocity [m/s];
W, mass flux [kg/s];
w, relative wave celerity [cm/s];
X, liquid concentration, kg solute/kg solvent; Lockhart–Martinelli parameter;
x, coordinate of flow direction;
x, mole fraction of CO_2 dimensionless;
Y, gas concentration, kg solute/kg solvent;
y, coordinate normal to flow direction.

Greek letters

α, pressure, factor [atm];
β, concentration factor [$kmol/m^3$];
Δ, increment, refers to length;
ε, eddy viscosity [m^2/h];
χ, wave number [cm^{-1}];

λ, λ', wavelength, [cm]; Baker factor;
μ, dynamic viscosity [kg/ms];
ν, kinematic viscosity [m^2/h];
ρ, density [kg/m^3];
σ, surface tension [g/s^2];
Φ, Lockhart–Martinelli parameter, velocity potential;
φ, central angle, radians; Kropholler–Carr factor;
ψ, Baker parameter;
ω, circular frequency [s^{-1}].

Subscripts

A, refers to air–ammonia–water system;
D, refers to carbon dioxide–water system;
G, gas phase;
H, refers to mass flux;
h, hydraulic value, refers to equivalent diameter;
i, i-th sample point;
L, liquid phase;
O, inlet conditions;
P, refers to air;
W, refers to water;
BM, refers to inert mean value;
pX, refers to pressure–X concentration system;
px, refers to pressure–x concentration system.

Superscripts

*, refers to equilibrium state;
-, mean-value.

INTRODUCTION

TWO-PHASE gas–liquid flow has been the subject of a great amount of research in the last 20 years.

Generally, these studies covered the dynamic behaviour of two-phase flow mixtures flowing in vertical or horizontal closed ducts. During the last 10 years the number of heat-transfer investigations of this system has increased because of the great importance of two-phase flow utilized as a coolant in power channels in the reactor core.

Mass transfer in two-phase flow studies has not been so popular as heat transfer investigations but now it is attracting more attention from investigators.

Among the latest investigations on mass transfer in horizontal two-phase flow the following works might be mentioned.

O'Brien and Stutzmann [1] obtained the mass transfer data in stratified smooth horizontal flow. Nesterenko [2] and Smolsky and Sergeev [3] published data on mass transfer in stratified flow with respect to gas side resistance. Anderson *et al.* [4] and Bollinger [5] investigated mass transfer during two-phase annular flow in a horizontal pipe for ammonia–air–water and carbon dioxide–water systems.

Heuss *et al.* [6] compiled data and correlations for horizontal froth flow of oxygen–water and ammonia–air–water systems.

Wales [7] did research on the absorption connected with chemical reaction in annular horizontal two-phase flow of carbon dioxide–water and carbon dioxide–alkali solution systems.

Mass transfer in two-phase horizontal bubble, slug, plug and annular flow were the subject of investigations published by Scott and Hayduk [8].

This short review of recent papers shows that the subject of most studies has been mass transfer in annular two-phase horizontal flow. Muenz and Marchello [9–11] studied mass transfer from a gas to the wave surface of water standing in a tank. They found the correlation for effective diffusity as a function of Schmidt and Reynolds numbers based on wave frequency.

Goren and Mani [12] checked the results of Muenz and Marchello. They presented a relation between the density of current difference (effective diffusity representative parameter) and frequency of waves (the authors used an electrolysis method for the mass-transfer prediction).

The purpose of the research described here was to find the correlations for mass-transfer coefficient in two-phase horizontal wavy flow and to verify the possibility of applying the mass-momentum analogy in this system.

THEORETICAL BACKGROUND

Flow dynamics

If a disturbance occurs on a free surface, it tends to produce a wave system.

The free surface condition with respect to the velocity potential is

$$\frac{\partial^2 \Phi}{\partial t^2} + g\frac{\partial \Phi}{\partial y} = 0. \tag{1}$$

Assuming an ideal motion on the x–y plane, we can use the second potential equation (Laplace equation)

$$\frac{\partial^2 \Phi}{\partial x^2} + \frac{\partial^2 \Phi}{\partial y^2} = 0. \tag{2}$$

Introducing two terms, one independent of space and the other of time, whose product is equal to potential function $\Phi(x, y, t)$, we can solve equation (1) by using the Laplace equation also. By considering the boundary conditions at the free surface and introducing the additional boundary conditions at the bottom of flow in the case of finite thickness d of liquid, we obtain the potential function expression

$$\Phi = A\cos(\chi x - \omega t)\cosh\chi(y + d). \tag{3}$$

Which represents the wave motion in the positive x direction with celerity

$$c = \frac{\omega}{\chi} = \left(\frac{g}{\chi}\tanh\chi d\right)^{\frac{1}{2}}. \tag{4}$$

Moreover, if we consider the effect of surface tension and liquid velocity (after dropping the density of gas ρ_G in the density difference and sum and density ration ρ_G/ρ_L), we obtain the more general form of celerity equation in two-phase flow

$$w = c - \bar{u}_L \approx \left[\left(\frac{g}{\chi} + \frac{\sigma\chi}{\rho_L}\right)\tanh\chi d\right]^{\frac{1}{2}}. \tag{5}$$

For very short waves and ripples, equation (5) is reduced to the form

$$w = \left(\frac{\sigma\chi}{\rho_L}\right)^{\frac{1}{2}} \tag{6}$$

but for waves moving on the surface of liquid with significant depth, equation (5) can be reduced to the expressions

$$w = (g\chi)^{\frac{1}{2}} \quad \text{for ratio} \quad \lambda/d < 2 \tag{7}$$

$$w = (gd)^{\frac{1}{2}} \quad \text{for ratio} \quad \lambda/d > 40. \tag{8}$$

The experimental results of investigations on wave dynamics in channels showed the difficulty of applying a highly developed theory of an ideal wave flow.

Recent investigations are connected with the stability approach theory of small disturbances. This theory, based on relations introduced by Orr [13] and Sommerfeld [14] has been developed in the last decade.

Simultaneously in recent years the wave flow in channels has been the subject of much experimental research such as that by Hanratty and Engen [15], Hanratty and Cohen [16, 17], Hanratty and Lilleleth [18, 19], Francis [20, 21], Keulegan [22], van Rossum [23], Del Bene [24], Ellis and Gay [25], etc.

Hanratty and Engen [15] introduced—according to their observations—three types of wave profiles. If gas velocity is increasing, the first so-called two-dimensional wave regime changes to the second three-dimensional one. The wave crests in this case are broken. If gas velocity is increased even more on the intersurface, the so-called roll waves, (moving ripples) are formed.

Surface between phases

Considered as if it were a sinusoidal wave profile, the expression of the intersurface is not very complicated, but the real wave profile differs appreciably from an ideal shape. In this case the surface between phases should only be defined as

$$A = \int b\sqrt{[(\mathrm{d}x)^2 + (\mathrm{d}y)^2]}. \tag{9}$$

Now assuming the wave surface place width in the tube to be constant and equal to mean value $\bar{b}$ (wave crests are below the tube axis) then equation (9) is

$$A = \bar{b}\int_0^l \sqrt{[1 + (dy/dx)^2]}\,.\,dx. \qquad (10)$$

By graphical differentiation of real wave profile, the total intersurface can be then predicted.

Mass transfer, gas film resistance

Let us consider an element of intersurface area having length dl_i. The lateral absorption rate is then

$$dW_A = K_G M_A \bar{\alpha}_i (Y_i - Y^*)\bar{b}dl_i \qquad (11)$$

where the pressure factor $\bar{\alpha}_i$ is defined as

$$\bar{\alpha}_i = (\bar{P} - \bar{p}_i)M_P/M_A. \qquad (12)$$

Note that the mass-transfer coefficient K_G in equation (11) is the so-called overall transfer coefficient. For the system discussed here it is approximately equal to the partial transfer coefficient k_G(here gas phase resistance).

We assume both coefficients to be equal. the error discussion about this assumption is presented in the Appendix.

The mass balance equation is

$$dW_A = W_G dY = W_L dX. \qquad (13)$$

Whereas the equations of equilibrium and operating lines are

$$Y^* = KX^* \qquad (14)$$

and

$$Y_i = -\frac{L}{G}X_i + Y_0 \qquad (15)$$

in the case of cocurrent gas and liquid flow.

By introducing relations (13)–(15) into relation (11), a differential equation is obtained, whose integration follows the expression for the mass transfer coefficient

$$k_G = \frac{W_L}{M_A \bar{\alpha}_{i+1}\bar{b}\Delta l_{i+1}\left(\frac{L}{G} + K\right)} \times \ln\left[\frac{Y_0 - \left(\frac{L}{G} + K\right)X_i}{Y_0 - \left(\frac{L}{G} + K\right)X_{i+1}}\right] \qquad (16)$$

where $\bar{\alpha}$ is calculated according to equation (12).

The values of the mean partial pressure $\bar{p}_i$ in equation (16) can be derived as the arithmetic mean of values of $\bar{p}_i$ and p_{i+1} calculated with the aid of the relation

$$p_i = \bar{P}\frac{M_P[Y_0 - (L/G)X_i]}{M_A + M_P[Y_0 - (L/G)X_i]}. \qquad (17)$$

In order to estimate the value of the mass-transfer coefficient, parameters W_L, W_G, Y_0, $\bar{P}$ and X_i are necessary and measurable. The width of the liquid stream $\bar{b}$ and the length increments Δl_i can be calculated by using the actual length of the wave profile obtained by graphical differentiation of the filmed profile.

Mass transfer, liquid film resistance

If mass transfer takes place between a pure active gas and flowing liquid, the lateral mass flux can be expressed as

$$dW_D = k_L \beta M_0 (X^* - X_i)\bar{b}dl_i. \qquad (18)$$

The equation of mass balance is

$$dW_D = W_i\,dX. \qquad (19)$$

The equilibrium relation between concentration in the liquid and overall pressure is

$$X^* = \frac{\bar{P}}{K_{px} - \bar{P}}\cdot\frac{M_D}{M_W}. \qquad (20)$$

Integration of the above equation (18) in conjunction with equations (19) and (20), follows the basic relation for mass transfer coefficient

$$k_L = \frac{W_i}{\beta M_D \Delta l_{i+1}\bar{b}}$$

$$\times \ln\left\{\frac{[\bar{P}/(K_{px}-\bar{P})]\dfrac{M_D}{M_W}-X_i}{[\bar{P}/(K_{px}-\bar{P})]\dfrac{M_D}{M_W}-X_{i+1}}\right\} \quad (21)$$

Parameters W_i, $\bar{P}$ and X_i can be measured experimentally. The values of Δl_i and $\bar{b}$ can be predicted as for gas film resistance.

Momentum–mass transfer analogy

When the fluid is in turbulent motion, the lateral flows of momentum, mass and heat are connected by equations based on the analogy between these lateral fluxes.

The equations representing the above analogy are the following

$$\frac{f}{2}=\frac{k}{\bar{u}}\left(\frac{v+\varepsilon}{E+D}\right)=\frac{h}{c\bar{u}\rho}\left(\frac{v+\varepsilon}{\bar{a}+E_H}\right). \quad (22)$$

Viscosity and diffusity ratios are expressed by rather complicated relations predicted by Prandtl [26], von Kármán [27], Martinelli [28], Boelter [29] and others, as functions of Schmidt, Reynolds and Prandtl numbers. The Reynolds [30] analogy assumes this function to be equal to unity.

We adopted the Kropheller and Carr [31] analogy. These authors introduced into the Reynolds analogy a specific factor φ, which corrects it. The relation for the factor φ is presented as a function of the Reynolds and the Schmidt, or Prandtl numbers.

The form of the analogy is

$$Sh=\frac{f}{2}\cdot\frac{1}{\varphi}\cdot\frac{d_{hG}\bar{u}_G}{D_G} \quad (23)$$

where

$$f=f(Re_G) \quad \text{and} \quad \varphi=f(Re_G, Sc).$$

EXPERIMENTAL

The horizontal test-section, shown in Fig. 1, was a 5 m long acrylic pipe 3 (see symbols in Fig. 1), 20 mm i.d. and 30 mm o.d., with seven liquid concentration taps, two pressure taps (at the test-section inlet and outlet) for pressure and pressure drop measurements, and two gas concentration taps. Each liquid and gas concentration tap was fitted with a copper–constantan thermocouple. All thermocouples were connected with the twelve point ekBT recorder. 2. The hot junctions of the thermocouples were

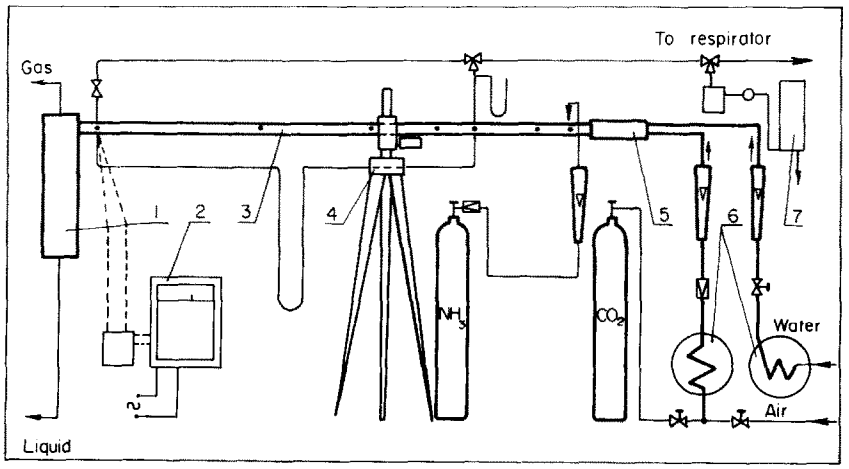

FIG. 1. Scheme of the test-apparatus. 1—separator, 2—recorder, 3—test-tube, 4—ciné camera, 5—mixer, 6—heaters, 7—interferometer.

protected with the aid of small polythene sheaths, to avoid corrosion effects.

Both phases—gas and liquid—passed through heaters 6, in which they reached the desired temperatures, and were metered to the test-section through rotameters.

In mixer 5 gas and liquid were mixed and entered the test-section.

The pipe calming section, in accordance with Kosterin's [32] data, was about 50 times i.d. in length.

Phases from the test-section were separated in separator 1 and passed out of the test section. A high-speed Pentaflex 16 camera 4 was installed in order to estimate wave profile, wave parameters, and surface between flowing phases. The film speed was about 100 frames per s, the exposure time being 1/1150 s.

The experimental procedure was divided into three periods. During the first, the desired conditions of flowrates, temperature, inlet concentration were achieved. In the second, in the steady state, the concentration liquid samples were taken, pressure drop estimated, concentration gas (in the case of air–ammonia gas phase) measured and flow profile recorded. During the third period, the liquid samples were titrated. Fluid temperatures were recorded during the whole time of the experiments so as to be sure of isothermal conditions. The liquid samples were sucked in 10 m small glass containers and then immediately injected into acid or base solution in excess, which was later titrated during the third period of experiment to obtain the exact concentration of ammonia or carbon dioxide in liquid.

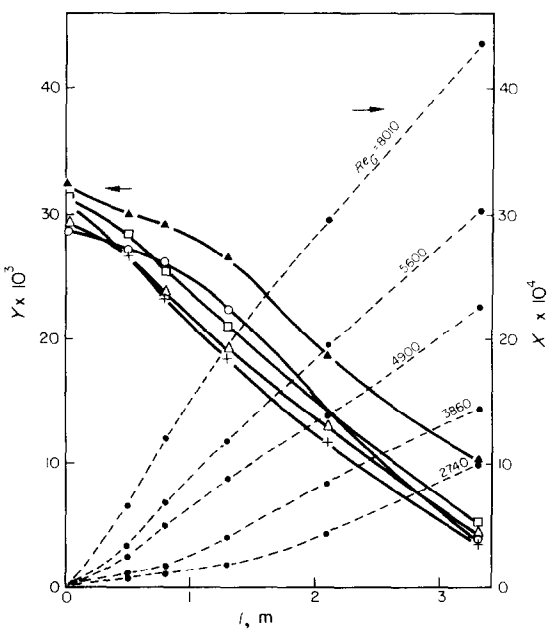

FIG. 2. Concentration (in kg per kg of pure solvent) distribution in gas and liquid phase along the channel. Ammonia–air–water system.

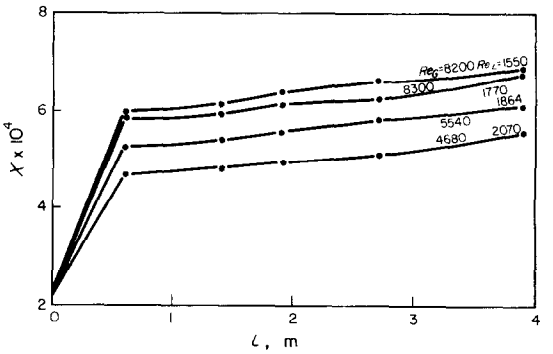

FIG. 3. Concentration (in kg per kg of water) distribution along the tube. Carbon dioxide–water system.

While investigating ammonia mass transfer during the second period of the experiment, gas concentration was measured to check liquid concentration predictions. Gas concentration was measured by means of a M 110 gas interferometer 7. Experimental data for mass transfer represent the concentration distribution in liquid along the pipe, under constant pressure and temperature conditions. Examples of this concentration distribution are shown in Fig. 2 for an air–ammonia–water system and in Fig. 3 for a carbon dioxide–water system. The discontinuity of concentration curves in Fig. 3 is due to different conditions for mass transfer at the inlet of the test section.

For the ammonia absorption experiments the ammonia was added to the air–water flow after

the mixer, at the inlet to the calming section, see Fig. 1. However, the two-phase carbon dioxide–water mixture was passed through the mixer.

The point $L = 0$ in the case of the ammonia absorption corresponds to the inlet of the calming section but in the case of the carbon dioxide absorption it corresponds to the inlet of the mixer.

RESULTS

Two-phase wavy flow dynamics. Surface prediction

The first experiments dealt with the comparison between the visually observed region of wavy flow and the predicted region according to Baker's [33] flow pattern correlation. The accuracy of Lockhart–Martinelli [34] correlation in wavy regime was checked as well.

In both cases a good agreement was found between the predicted and experimentally obtained values of flowrate regime and the Lockhart–Martinelli parameters (for turbulent flow in both phases). Figure 4 shows the Lockhart–Martinelli curves and experimentally predicted points.

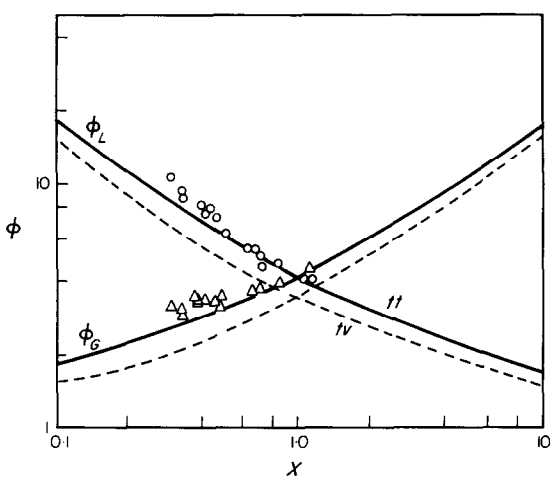

FIG. 4. Comparison between experimentally obtained data of pressure drop and Lockhart–Martinelli correlation (tt—refers to turbulent motion in both phases; tv—refers to turbulent motion in gas phase and laminar in liquid phase).

An analysis of the wave profiles recorded on the films enabled us to determine the enlargement of the flat surface in the presence of wave disturbances and to predict some relations between flow and wave parameters. Generally, the intersurface increase proved not to be significant. In a few cases only the so-called increase surface ratio $\Delta l/l$, which was defined as the ratio (in per cent) between difference of length along wave curvature and length of pipe to length of pipe, was higher than 6 per cent. The length ratio was taken as a mean value of some profile set data for the same flow conditions.

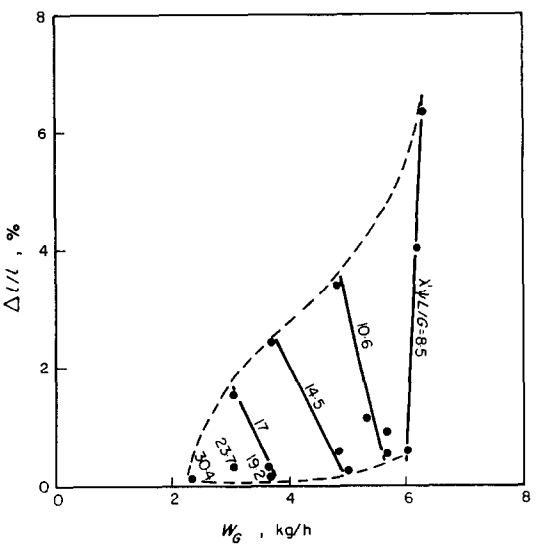

FIG. 5. Length increment ratio vs. gas flowrate.

Figure 5 shows the plot for air ammonia–water data. Dash lines represent the limit of the wave region and terminate at the onset of other regimes of two-phase flow. It can be observed that only a very small change in gas velocity causes significant variation in the length ratio.

Generally, with the increase of the Baker two-phase flow ratio $\lambda'\psi L/G$, and the length of wave λ, the length ratio $\Delta l/l$ decreases, as observed in Fig. 6.

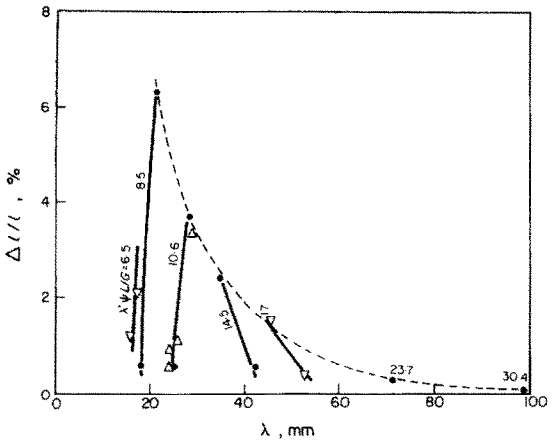

FIG. 6. Length increment ratio against wavelength.

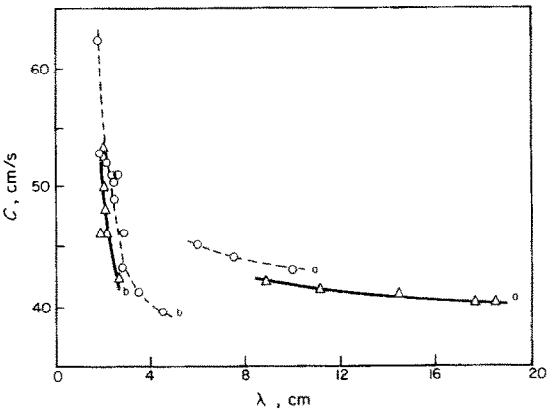

FIG. 8. Wave celerity vs. wavelength. Dashed lines: air–water system, continuous lines: carbon dioxide–water system.

The margin of $\Delta l/l$ ratio for lower values of wave lengths and flow ratios increases very markedly, thus achieving a 6 per cent value at the lowest flow ratio $\lambda'\psi L/G$ equal to 8·5.

The verification of the type of wave regions based on scrupulous analysis of flow patterns showed a very good agreement with wave regimes observed and defined by Hanratty and Engen [15]. All three types of waves were observed in experiments.

Figure 7 shows the plots of wave variation celerity against the Reynolds number for air–water and carbon dioxide–water systems. This variation can be divided into two parts. One corresponds to the so-called two-dimensional waves with significant wavelength, the other corresponds to the three-dimensional waves. For the highest values of the Reynolds number the latter curves pass through roll-wave regime and terminate at the onset of slug flow regime. The same trend of variation can be observed in the celerity vs. wavelength plot of Fig. 8.

The curves (dashed for air–water system; continuous for carbon dioxide–water system)

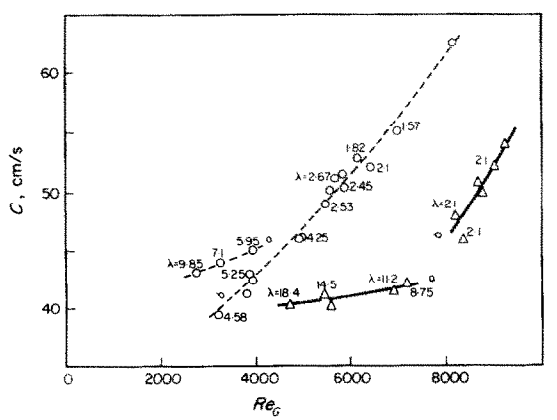

FIG. 7. Wave celerity as a function of gas Reynolds number. Dashed lines correspond to air–water system, continuous lines to carbon dioxide–water system.

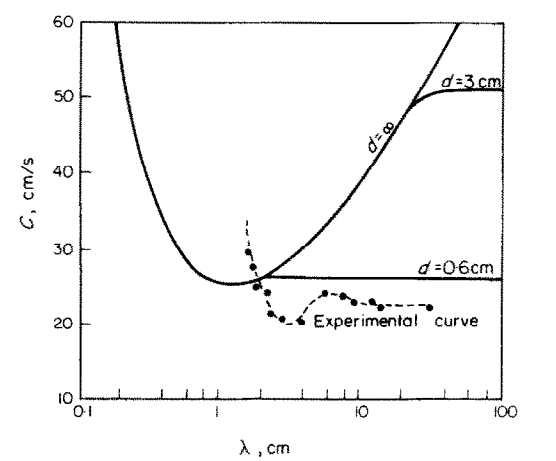

FIG. 9. Comparison between experimentally obtained and theoretically calculated data of celerity vs. wavelength relation.

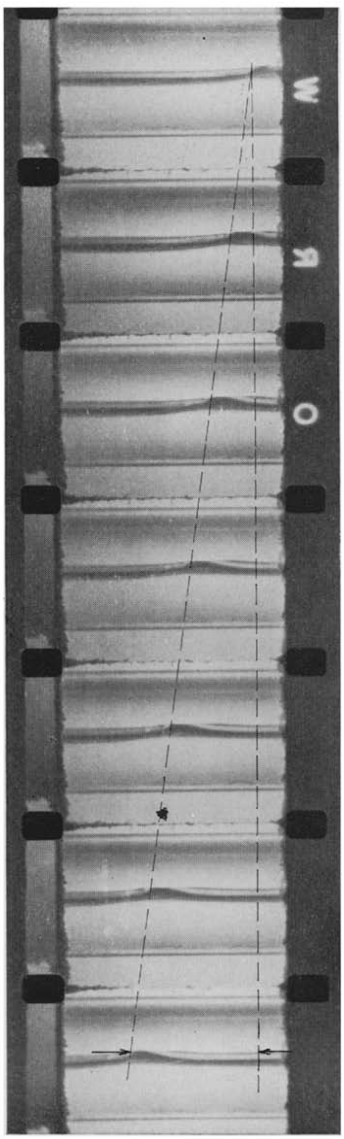

FIG. 10. Wave celerity determination on film frames.

[facing page 1268]

a correspond to two-dimensional long waves and b to three-dimensional and roll-waves.

The qualitative comparison between experimentally obtained variation of celerity against wavelength is shown in Fig. 9 in semilogarithmic coordinates: the trend of both curves is very similar and one for selected equivalent depth (i.e. 0·6 cm) of water the difference between curves is not very great for celerity but it is for wavelength values in the short wave region. In all cases, the celerity of waves was predicted as a ratio of distances between moving tops of wave crests on the two neighbouring film frames and the time constant of film velocity (~0·01 s) as shown in Fig. 10.

MASS TRANSFER

As mentioned above, the mass transfer coefficient in an air–ammonia–water system was calculated according to equation (16) after the substitution of measured parameters such as: flowrates, pressure, intersurface length, concentrations. Calculations were performed on the EMC-Gier computer. About 500 values of gas film mass-transfer coefficient were obtained for Reynolds numbers ranging between 2500 and 8000.

In order to estimate the correlations of dimensionless moduli, Sherwood, Reynolds and Schmidt numbers were calculated.

The definitions of these numbers are as follows:

The Sherwood number

$$Sh_h = \frac{k_G \bar{p}_{BM} R T d_{hG}}{D_G \bar{P}} \tag{24}$$

where $\bar{p}_{BM}$ is the logarithmic mean of inert partial pressure and the equivalent diameter is

$$d_{hG} = d\,\frac{\varphi_G - \sin(\varphi_G/2)}{\varphi_G + 2\sin(\varphi_G/2)} \tag{25}$$

with equality

$$\varphi_G = 2\pi - \varphi_L.$$

The Reynolds numbers

$$Re_G = \frac{(\bar{u}_G - \bar{u}_L)\rho_G d_{hG}}{\mu_G} \tag{26}$$

and

$$Re_F = \frac{(\bar{u}_G - c)\rho_G d_{hG}}{\mu_G}. \tag{27}$$

The Schmidt number

$$Sc = \frac{\mu_G}{\rho_G D_G}. \tag{28}$$

The mean central angle φ_L of water stream width on the intersurface was determined simultaneously with the intersurface analysis of profile frames. Values of Sherwood and Reynolds numbers calculated in this way were used to predict the correlation for gas film mass-transfer coefficient by means of the least squares method.

As a result of calculations performed also on the EMC-Gier computer, we obtained:

the so-called slip correlation

$$Sh_h = 0{\cdot}289 \,.\, 10^{-4}\, Re_G^{1{\cdot}615} \,.\, Sc^{0{\cdot}5} \tag{29}$$

which is given in Fig. 11 and

the slip-wave correlation

$$Sh_h = 0{\cdot}3 \,.\, 10^{-4}\, Re_F^{1{\cdot}46} \,.\, Sc^{0{\cdot}5}. \tag{30}$$

The value of Schmidt number power (0·5) was taken from literature data [35, 36, 37 etc.]

The correlation between dimensionless numbers for liquid film mass-transfer coefficient was obtained in a similar way.

For mass-transfer coefficient determination, equation (21) was used and all measured parameters were substituted in it (flowrates, pressure, liquid concentrations actual length of the intersurface).

The definitions of Sherwood and Reynolds numbers are

$$Sh_h = \frac{d_{hL} k_L}{D_L} \tag{31}$$

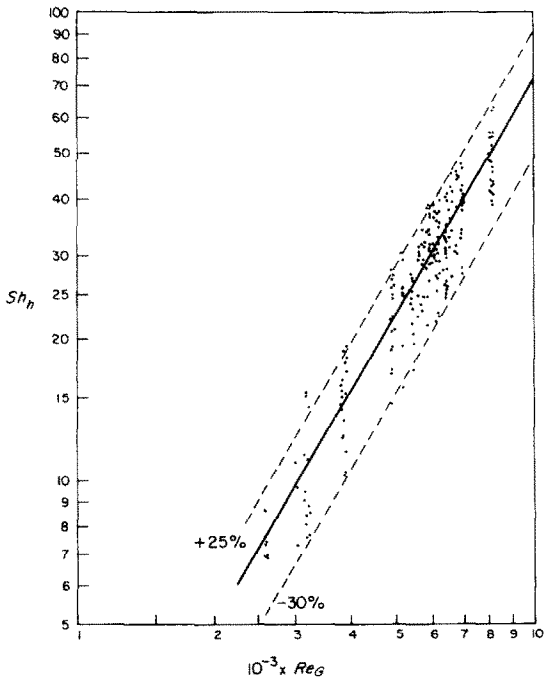

FIG. 11. Mass-transfer data for ammonia–air–water system. Correlation of Sherwood and Reynolds numbers.

where equivalent diameter d_{hL} was calculated according to equation (25) after the substitution of central angle φ_L and

$$Re_L = \frac{\bar{u}_L d_{hL} \rho_L}{\mu_L}. \tag{32}$$

In the case of liquid film resistance, nearly 300 values of mass-transfer coefficient were obtained from the 1200–2400 range of Reynolds numbers. The correlation was obtained by means of the least squares method carried out on the EMC–Gier computer.

The Schmidt number power was estimated by experiments carried out at various temperatures; the temperature range was 15–30°C. The final equation is the following

$$Sh_h = 0{\cdot}00413 \,.\, Re_L^{0{\cdot}916} \,.\, Sc^{0{\cdot}5}. \tag{33}$$

Momentum–mass transfer analogy

The analogy between mass and momentum fluxes was only applied to gas film mass-transfer resistance analysis.

In order to estimate the Sherwood number in this way [according to expression (23)], the values of friction factor f on the rough wave surface were required. Smith and Tait [38] and Hanratty and Cohen [17] reported the experimental data about this factor as a function of gas velocity and Reynolds number. At first, the friction factor increases with gas velocity up to the point where it starts becoming constant.

Both the above mentioned data were used to calculate the Sherwood numbers for corresponding Reynolds numbers of gas flow.

Figure 12 shows the curves representing relations calculated with respect to mass momentum analogy. Line d corresponds to Smith and Tait data, line a to Hanratty and Cohen data,

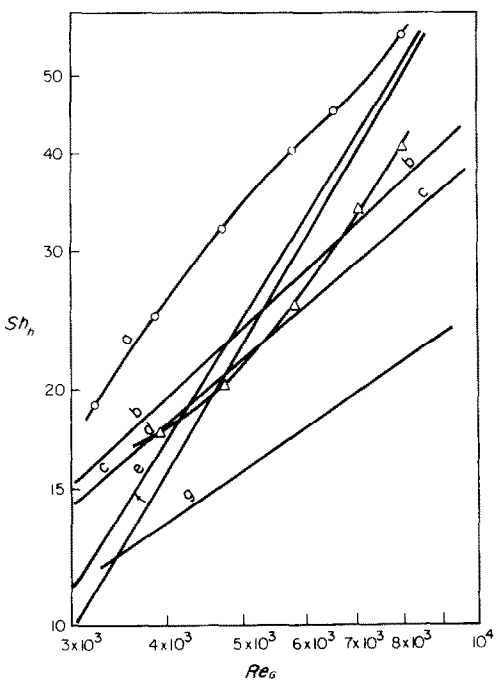

FIG. 12. Comparison between data of mass transfer obtained in experiments and predicted by means of mass-momentum analogy for air–ammonia–water system.

whereas line f is related to equation (29) and line e to equation (30). In Fig. 12 there are also plotted correlation curves for stratified two-phase flow [39] and the well known van Krevelen, Hoftijzer [40] and Gilliland and Sherwood [41] correlations for wetted wall columns (lines b and c).

DISCUSSION

Comparison between curves plotted in Fig. 12 shows a very good agreement between experimentally obtained values of Sherwood numbers, calculated on the basis of mass–momentum analogy.

For high Reynolds numbers the experimentally predicted curves pass almost exactly between two lines obtained from friction factor data. Moreover, in this part of the plot the slope of mentioned curves is almost identical. For lower Reynolds numbers (3000–4000) the values of Sherwood numbers are almost equal to values obtained experimentally by Buzek [39] —correlation line g in Fig. 12—in the case of the stratified two-phase flow.

In this region two-phase wavy flow had the form of very long (about 15 cm), two-dimensional smooth waves. The roughness of their smooth wave surface did not differ greatly from the roughness of a water flat surface. Thus, the values of mass-transfer coefficient and the Sherwood numbers should be almost identical for both the wave and stratified regions. The lines related to wetted-wall column data by van Krevelen and Gilliland pass through the central part of the plots obtained in our research. The difference of Sherwood numbers for both ends of the above plots is due to the different mechanism of wavy flow in the case of horizontal and vertical flows. It consists of different types of originating waves ripples and so-called horizontal shallow-water waves) and water stream depths. But this difference is not so great as appears from van Krevelen or Gilliland data. For ammonia absorption in a wetted-wall column, Ramm *et al.* [42] recently reported a correlation with the Reynolds number power equal to 1·32 (being the slope of the correlation line) in comparison with our predicted value equal to 1·5–1·6.

Data obtained for liquid film mass-transfer resistance do not differ very much from stratified flow data [43], but are about five times lower than wetted wall column data. Table 1 gives the comparison between cited [43] data and our predicted data.

Table 1

Reynolds number*	1400	1600	1800	2000	2200
K_L predicted [m/h]	0·060	0·070	0·076	0·084	0·092
K_L cited [43] [m/h]	0·049	0·057	0·059	0·063	0·067

K_L calculated for $d_{hL} = 0{\cdot}008$ m.

Muenz and Marchello [11] found that effective diffusity increases 1030 per cent with respect to flat surface diffusion if the frequency of waves being originated on the surface increases by 400–1000 cycles per min. In our research the frequency changed from 150 to 1500 cycles per min. As observed in Table 1 the difference between our mass transfer coefficient data and reported flat surface data [43] varies from 20 per cent ($Re = 1400$, frequency = 150) to 37 per cent ($Re = 2200$, frequency = 1500). There seems to be a rather good agreement between Muenz–Marchello's and our data.

CONCLUSIONS

As a final result of this research, the following conclusions can be drawn:

1. Two-phase wavy horizontal flow pattern and pressure drop can be predicted with good agreement by the Baker [33] and Lockhart–Martinelli [34] correlations.
2. The presence of wave disturbance in the intersurface usually causes a small percentage increase of surface area.

* Reynolds number is calculated from equation (32).

3. The mass-transfer coefficients for both cases of mass-transfer resistances can be estimated with the aid of correlations (29) and (33) predicted in this research.

4. The presence of small wave disturbances on the intersurface essentially intensifies lateral mass flux for both cases of mass-transfer resistances.

5. A good agreement was found between experimentally obtained results and results calculated by momentum–mass analogy based on experimental friction factor data [17, 38].

6. The application of wetted-wall vertical column transfer data for horizontal two-phase wavy flow is rather unsuccessful.

REFERENCES

1. L. O'Brien and L. Stutzmann, Mass transfer of pure liquids from a plane, free surface, *Ind. Engng Chem.* **42**, 1181 (1950).
2. A. Nesterenko, Heat and mass transfer in free surface liquid evaporization, *Z. Tech. Fiz.* **24**, 729 (1954).
3. B. Smolsky and G. Sergeev, Heat and mass transfer with liquid evaporation, *Int. J. Heat Mass Transfer* **5**, 1011 (1962).
4. J. D. Anderson and R. E. Bollinger, Gas phase controlled mass transfer in two-phase annular horizontal flow, *A.I.Ch.E.Jl* **10**, 640 (1964).
5. R. E. Bollinger, M.S. Thesis, University of Delaware (1960).
6. J. M. Heuss, C. J. King and C. R. Wilke, Gas liquid mass transfer in cocurrent froth flow, *A.I.Ch.E.Jl* **11**, 866 (1965).
7. C. E. Wales, Physical and chemical absorption in two-phase annular and dispersed horizontal flow, *A.I.Ch.E.Jl* **12**, 1166 (1966).
8. D. S. Scott and W. Hayduk, Gas absorption in horizontal cocurrent bubble flow, *Can. J. Chem. Engng* **44**, 130 (1966).
9. K. Muenz and J. M. Marchello, Technique for measuring amplitude of small surface waves, *Rev. Scient. Instrum.* **35**, 953 (1964).
10. K. Muenz, Ph. Thesis, University of Maryland (1965).
11. K. Muenz and J. M. Marchello, Surface motion in gas absorption, *A.I.Ch.E.Jl* **12**, 249 (1966).
12. S. L. Goren and R. V. S. Mani, Mass transfer through horizontal liquid films in wavy motion, *A.I.Ch.E.Jl* **14**, 57 (1968).
13. W. Orr, *Proc. R. Irish Acad.* **17(A)**, 124 (1907).
14. A. Sommerfeld, Atti del Congr. Intern. dei Mat. Roma (1908).
15. 15. T. J. Hanratty and J. M. Engen, Interaction between a turbulent air stream and a moving water surface, *A.I.Ch.E.Jl* **3**, 299 (1957).
16. T. J. Hanratty and L. S. Cohen, Genrations of waves in the cocurrent flow of air and a liquid, *A.I.Ch.E.Jl* **11**, 138 (1965).
17. T. J. Hanratty and L. S. Cohen, Effect of waves at a gas–liquid interface on a turbulent air flow, *J. Fluid Mech.* **31**, 467 (1968).
18. T. J. Hanratty and L. U. Lilleleth, Measurement of interfacial structure for cocurrent air–water flow, *J. Fluid Mech.* **11**, 65 (1961).
19. T. J. Hanratty and L. U. Lilleleth, Relation of the interfacial shear stress to the wave height for cocurrent air–water flow, *A.I.Ch.E.Jl* **7**, 548 (1961).
20. J. R. D. Francis, The aerodynamic drag of free water water surface, *Proc. R. Soc., Lond.* **206A**, 387 (1951).
21. J. R. D. Francis, Wave motion and the aerodynamic drag, *Phil. Mag.* **45**, 695 (1954).
22. G. H. Keulegan, Wind tides in small channels, *J. Res. Natn. Bur. Stand.* **46**, 358 (1951).
23. J. J. Van Rossum, Experimental investigation of horizontal liquid film on a free oil surface, *Chem. Engng Sci.* **11**, 35 (1959).
24. J. Del Bene, Stability theory applied to wave formation in a parallel gas–liquid flow, Ph.D. Thesis, Purdue University (1965).
25. S. R. M. Ellis and B. Gay, The parallel flow of two fluid streams: interfacial shear fluid–fluid interaction, *Trans. Inst. Chem. Engrs* **37**, 206 (1959).
26. L. Prandtl, Eine Beziehung zwischen Wärmeaustausch und Strömungwiederstand der Flüssigkeiten, *Physik Z.* **11**, 1072 (1910) and Bemerkung über den Wärmeübergang im Rohr **29**, 287 (1928).
27. Th. Von Kármán, The analogy between fluid fraction and heat transfer, *Trans. Am. Soc. Mech. Engrs* **61**, 705 (1939).
28. R. C. Martinelli, Heat transfer to molten metals *Trans. Am. Soc. Mech. Engrs* **69**, 947 (1941).
29. L. M. K. Boelter, R. C. Martinelli and F. Jonassen, Remarks on the analogy between heat transfer and momentum transfer, *Trans. Am. Soc. Mech. Engrs* **63**, 447 (1947).
30. O. Reynolds, On the extent and action of the heating surface of steam boilers, *Proc. Lit. Phil. Soc., Manchester* **14**, 7 (1874).
31. H. W. Kropholler and A. D. Carr, The prediction of heat and mass transfer coefficients for turbulent flow in pipes at all values of the Prandtl and Schmidt number, *Int. J. Heat Mass Transfer* **5**, 1191 (1962).
32. S. Kosterin, Investigation of pipe position and diameter influence on hydraulic friction and flow structure of flowing gas–liquid mixture, *Izv. Acad. Nauk. SSSR, Ot'del. Tek. Nauk.* **12**, 1824 (1949).
33. O. Baker, Simultaneous flow of oil and gas, *Oil Gas J.* **53**, H12, 185 (1954).
34. R. W. Lockhart and R. C. Martinelli, Proposed correlation of data for isothermal two-phase, two-component flow in pipes, *Chem. Engng Prog.* **45**, 39 (1949)
35. G. A. Morris and J. Jackson, *Absorption Towers.* Butterworth, London (1953).
36. V. Maljusov, Ph.D. Thesis, Fiz. Khim. Inst. Karpova, Moscow (1951).

37. N. ZHAVORONKOV, S. KRASHENINNIKOV and J. FURMIER, *Trudy. M. Ch. T.I.* **18**, 95 (1954).
38. T. N. SMITH and R. W. F. TAIT, Interfacial shear stress and momentum transfer in horizontal gas–liquid flow, *Chem. Engng Sci.* **21**, 63 (1966).
39. J. BUZEK, Private communication, Conf. of Chem. Eng. and Chem. Ap. Łódź, Poland (1968).
40. D. W. VAN KREVELEN and P. J. HOFTIJZER, Studies of gas absorption; mass transfer in film reactors (wetted wall columns), *Rec. Trav. Chim.* **68**, 221 (1949).
41. E. GILLILAND and T. SHERWOOD, Diffusion of vapors into air streams, *Ind. Engng Chem.* **26**, 516 (1934).
42. V. RAMM, N. CHERTKOV and N. DOBROMYSLOVA, Absorption of NH_3 by water and sulfuric acid, *Z. Prik. Khim.* **38**, 1972 (1965).
43. M. JAROSZYŃSKI, Private communication, Conf. of Chem. Eng. and Chem. Ap., Łódź Poland (1968).

APPENDIX

It was observed in previously published data that liquid film resistance in the case of ammonia absorption in water is rather significant. Because of this, we estimated the error made by introducing the assumption of negligible liquid phase resistance. Diffusion properties of carbon dioxide and ammonia in water are almost identical, for instance: at 20°C, diffusities and Schmidt numbers for CO_2 and NH_3 are as follows

$$D_{NH3} = 0{\cdot}637 \text{ m}^2/\text{h}, \quad Sc = 568$$

$$D_{CO2} = 0{\cdot}634 \text{ m}^2/\text{h}, \quad Sc = 570.$$

From the above, the liquid transfer coefficient for both absorption systems should be nearly the same.

The overall mass-transfer coefficient is defined

$$\frac{1}{K_G} = \frac{1}{k_G} + \frac{1}{H \cdot k_L} \cdot \frac{R_L}{R_G} \tag{A.1}$$

where $H = c/p$.

For extreme cases of ammonia–air–water system dynamics, experimentally estimated values of k_L and k_G were introduced into the equation for K_G, and the maximum error (second group of the right-hand side of equation (A1) was found to be only 7·7–8 per cent of K_G value).

TRANSFERT MASSIQUE DANS UN ÉCOULEMENT BIPHASIQUE GAZ–LIQUIDE À SURFACE ONDULÉE

Résumé—Le transfert massique dans un écoulement biphasique gaz–liquide dans un tube circulaire fait l'objet de cette étude.

On obtient les coefficients de transfert massique pour des résistances de film gaz et liquide.

L'analogie masse-quantité de mouvement basée sur des résultats expérimentaux de coefficient de frottement en surface ondulée est utilisée pour déterminer les coefficients de transfert massique.

Une comparaison est faite entre les coefficients de transfert massique expérimentaux et les résultats obtenus par la méthode analogique.

Quelques expériences sur la dynamique et la géométrie de l'écoulement avec ondulation sont aussi conduites.

STOFFÜBERGANG IN ZWEIPHASIGER GAS–FLÜSSIGKEITS–WELLENSTRÖMUNG

Zusammenfassung—Die Stoffübertragung bei horizontaler Zweiphasen-Wellenströmung (gasförmig–flüssig) im runden Rohr ist Gegenstand der vorliegenden Untersuchung. Es wurden experimentell Beziehungen für die Stoffübergangskoeffizienten für Gas- und Flüssigkeitsoberflächen ermittelt. Außerdem wurde die Analogie zwischen Stoff- und Impulsaustausch benutzt, um die Stoffübertragungskoeffizienten zu bestimmen, wobei experimentelle Daten von Schubspannungen für die wellige Oberfläche zugrunde lagen.

Es wurden die experimentellen Werte der Stoffübergangskoeffizienten mit den Werten der Analogiemethode verglichen. Ausserdem werden einige Experimente über die Dynamik und Geometrie der Wellenströmung durchgeführt.

МАССООБМЕН В ДВУХФАЗНОМ ГАЗО-ЖИДКОСТНОМ ВОЛНОВОМ ТЕЧЕНИИ

Аннотация—Предметом исследования был массообмен между горизонтальным двухфазным газо-жидкостным волнообразнодвижущимся потоком и круглой трубой. Экспериментально получены корреляции коэффициентов массообмена для сопротивления газа и жидкой пленки. Для определения коэффициентов массообмена использовалась аналогия между переносом массы и количества движения, основанная на

экспериментальных данных о коэффициенте трения волнистой поверхности. Проведено сравнение коэффициентов массообмена, полученных экспериментально и по методу аналогии. Проведены также некоторые эксперименты по геометрии и гидродинамике волнообразного течения.